Transformer-Coupled Multiport ZVS Bidirectional DC–DC Converter With Wide Input Range

Haimin Tao, Andrew Kotsopoulos, Jorge L. Duarte, *Member, IEEE*, and Marcel A. M. Hendrix, *Member, IEEE*

***Abstract*—Multiport dc–dc converters are particularly interesting for sustainable energy generation systems where diverse sources and storage elements are to be integrated. This paper presents a zero-voltage switching (ZVS) three-port bidirectional dc–dc converter. A simple and effective duty ratio control method is proposed to extend the ZVS operating range when input voltages vary widely. Soft-switching conditions over the full operating range are achievable by adjusting the duty ratio of the voltage applied to the transformer winding in response to the dc voltage variations at the port. Keeping the volt-second product (half-cycle voltage-time integral) equal for all the windings leads to ZVS conditions over the entire operating range. A detailed analysis is provided for both the two-port and the three-port converters. Furthermore, for the three-port converter a dual-PI-loop based control strategy is proposed to achieve constant output voltage, power flow management, and soft-switching. The three-port converter is implemented and tested for a fuel cell and supercapacitor system.**

***Index Terms*—Bidirectional converters, fuel cells, multiport converters, soft-switching, supercapacitors, three-port converters.**

I. Introduction

MULTIPORT converters, a promising concept for alternative energy systems, have attracted increasing research interest recently [1]–[8]. Compared with the conventional approach that uses multiple converters, a multiport converter promises cost-effective, flexible, and more efficient energy processing by utilizing only a single power stage.

For dc–dc power conversion, the dual-active-bridge (DAB) converter (Fig. 1) has been proposed in [9]. It has attractive features such as low device stresses, bidirectional power flow, fixed-frequency operation, and utilization of the transformer leakage inductance as the energy transfer element. The main drawback of the DAB converter, however, is that it cannot handle a wide input voltage range (e.g., fuel cells and supercapacitors). In such a case the soft-switching region of operation will be significantly reduced [9], [10].

Manuscript received July 19, 2005; revised April 27, 2007. This work was supported by the Dutch funding agency for university research—the technology foundation STW. Recommended for publication by Associate Editor K. Ngo.

H. Tao was with the Electrical Engineering Department, Eindhoven University of Technology, Eindhoven 5600 MB, The Netherlands and is now with Philips Lighting B.V., Eindhoven 5600, The Netherlands (e-mail: haiman.tao@gmail.com)

J. L. Duarte and M. A. M. Hendrix are with the Electrical Engineering Department, Eindhoven University of Technology, Eindhoven 5600 MB, The Netherlands (e-mail: j.l.duarte@tue.nl; m.a.m.hendrix@tue.nl).

A. Kotsopoulos is with the ANCA Pty., Ltd., Bayswater North VIC 3153, Australia (e-mail: andrewk@anca.com.au).

Digital Object Identifier 10.1109/TPEL.2007.915129

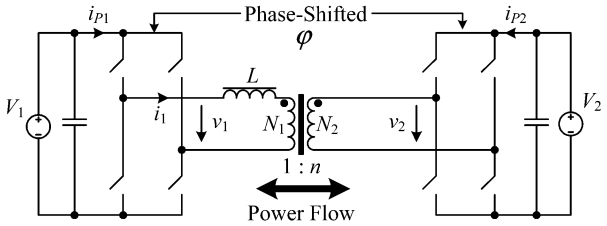

Fig. 1. Dual-active-bridge (DAB) converter topology.

As an extension of the DAB topology, a three-port triple-active-bridge (TAB) converter for a fuel cell and battery system was proposed in [11]. A similar topology was found in [12] for the application of uninterrupted power supply (UPS) systems. However, like the DAB converter, the TAB converter does not maintain ZVS when wide voltage variations are present.

To extend the soft-switching operating range, an inductor can be paralleled to the transformer; however, it will not extend the ZVS area to 100% [13]. References [13] and [14] have proposed a voltage cancellation method, effectively a form of duty ratio control, along with phase shift control to extend the ZVS operating region. The method uses an offline calculated lookup table of the control angles with the output current and voltage (V-I plane) as the look-up parameters. The goal is to control the delay angle of the firing signal of one of the bridge legs, and therefore the zero-crossing of the current, such that all the switches are soft-switched. However, the described method is complex to implement and equations for calculating the angles have not been published. Duty ratio control was also used in [12] for adjusting the amplitude of the fundamental component, but not explicitly for extending the ZVS range. In addition, a phase shift plus pulse-width-modulation (PWM) control was applied to the DAB converter in [15], where the converter uses two half-bridges to generate asymmetrical waveforms in order to deal with the voltage variation. However, for the multiport topologies, with this method only one port may have a wide operating voltage because all the bridges operate at the same duty ratio.

Using a Δ-equivalent model of the transformer network to analyze the power flow in a three-port system has been discussed in [11] and [16]. This approach simplifies the analysis of the power flow.

For the TAB converter duty ratio control can be used to compensate for voltage variations at the ports. We propose that the duty ratio is imposed according to the operating voltage of the port, being inversely proportional. In this way the effective voltages (volt-second products) presented to the transformer windings are equal (i.e., their half-cycle voltage-time integrals are

equal). In multiport topologies it is therefore possible to extend the ZVS operating range to the entire operating region. Note that although both are a form of duty ratio control, the proposed method (keeping the volt-seconds equal) is different from the method presented in [13] and [14]. The way in which the duty ratio is controlled is essentially different.

An embodiment of the idea is a fuel cell system using a three-port converter. The implementation of a fuel cell system needs energy storage to improve the system dynamics. A supercapacitor has an advantage over batteries in terms of transient energy storage because it can be recharged and discharged virtually unlimited times, and the state-of-charge (SOC) of a supercapacitor is simply a function of the voltage. However, the supercapacitor operating voltage varies widely compared with batteries. To keep ZVS, duty ratio control is applied to the supercapacitor bridge.

This paper elaborates on our previous work in [17] and [18]. Presented in the following sections are the ZVS analysis for the DAB and TAB converters, the system modeling, dual-PI-loop control strategy, soft start-up methods, as well as simulation and experimental results.

II. Two-Port Topology

A. DAB Converter With Duty Ratio Control

In the conventional DAB converter (Fig. 1), each bridge generates a square-wave voltage. The two voltages v_1 and v_2 are phase-shifted with respect to each other with an angle φ to control the amount of power flow through the inductor L which represents the sum of the primary-referred transformer leakage inductance and optional external inductor.

The DAB converter suffers from a limited soft-switching range if the port dc voltages change dynamically in a relatively wide range [9]. Fig. 2 plots the soft-switching (SS) region of the DAB converter, showing the dependence of the ZVS range on the dc conversion ratio d which is defined as $d = V_2/(nV_1)$, where $n = N_2/N_1$ is the transformer turns ratio. The power flow in the figure is expressed in per unit (p.u.) with the base defined as $P_B = V_1^2/(\omega L)$, where $\omega = 2\pi f_s$ (f_s is the switching frequency in Hz). For the V_1-side bridge, hard-switching (HS) can occur when $d > 1$. Under idealized conditions the soft-switching operating range can be calculated by solving for the current at the switching instances and enforcing the ZVS constraints, i.e., a positive current through the outgoing power switch. This is found to be

$$|\varphi| > \frac{\pi}{2}\left(1 - \frac{1}{d}\right). \tag{1}$$

For the V_2-side bridge hard-switching can occur when $d < 1$, and the soft-switching operating range is

$$|\varphi| > \frac{\pi}{2}(1 - d). \tag{2}$$

For a given d, the minimum operating phase shift which results in soft-switching can then be determined. Full control range under soft switching is achievable for $d = 1$. In general, the larger the phase shift, the better the switching condition.

In addition to the phase shift control, this paper introduces a simple duty ratio control method to extend the ZVS range.

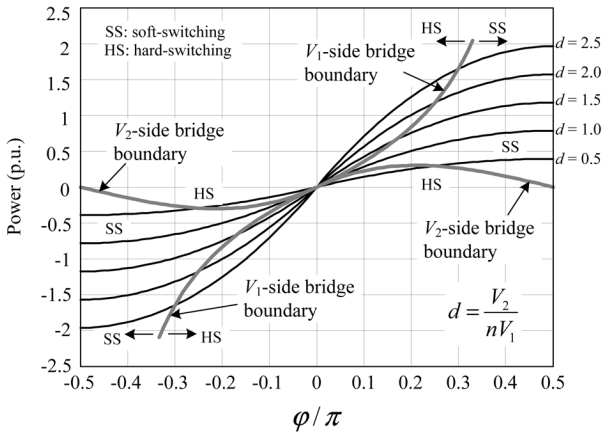

Fig. 2. Soft-switched operating region of the conventional DAB converter.

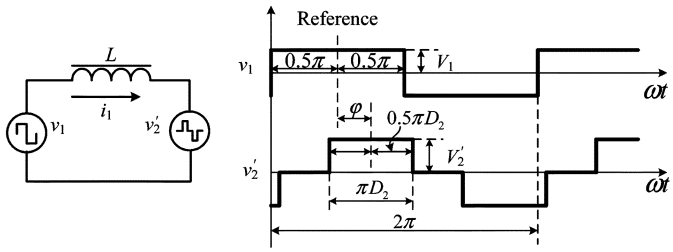

Fig. 3. Fundamental model of the DAB converter with phase shift φ and duty ratio control. V_2 and v_2 are referred to the primary (V_1) side and represented by V_2' and v_2', respectively. D_2 denotes the duty ratio of v_2'.

The definition of the duty ratio is shown in Fig. 3. It represents the pulse width of the rectangular-pulse-wave and has a value between 0 and 1 (1 for square-wave). In Fig. 1 the voltage source V_1 is assumed to be constant; thus the V_1-side bridge operates in square-wave mode (i.e., $D_1 = 1$), whereas V_2 varies between its minimum voltage $V_{2\min}$ and the maximum voltage $V_{2\max}$. We calculate the duty ratio as

$$D_2 = \frac{V_{2\min}}{V_2}. \tag{3}$$

According to (3), the duty ratio is inversely proportional to the voltage. If V_2 equals $V_{2\min}$, then $D_2 = 1$. A larger value of V_2 results in a smaller duty ratio. The transformer turns ratio n is chosen according to

$$n = \frac{N_2}{N_1} = \frac{V_{2\min}}{V_1}. \tag{4}$$

Then, D_2 can also be expressed as

$$D_2 = \frac{nV_1}{V_2}. \tag{5}$$

The phase shift φ, as shown in Fig. 3, is imposed with respect to the central axis of the voltage pulse (i.e., the phase shift between the fundamental components). The phase shift is positive when v_1 leads v_2, resulting in a power flow from V_1 to V_2. A negative phase shift means that v_2 leads v_1, and power flows from V_2 to V_1.

The volt-second product is defined as the time integral of a half-cycle of the winding voltage. For a rectangular-pulse-wave

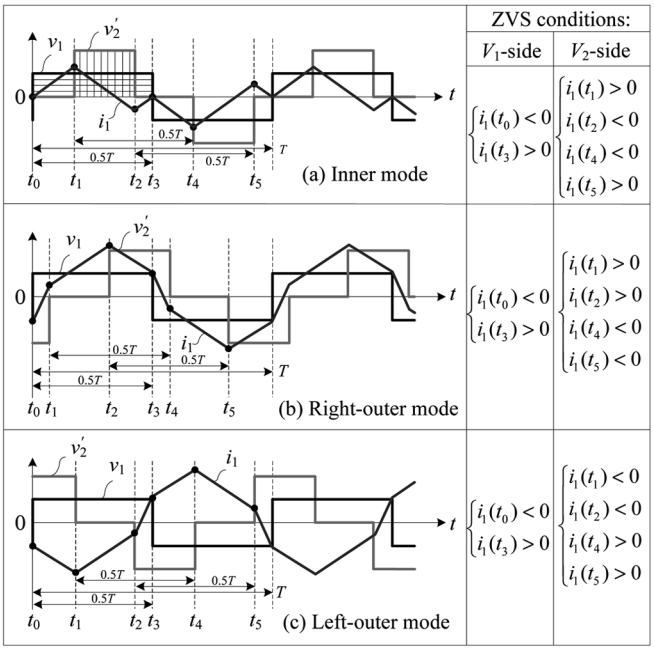

Fig. 4. Possible operation modes at different phase shifts: (a) inner mode, and (b) and (c) outer mode. The shaded areas represent the volt-seconds of v_1 and v_2'.

voltage the integral simplifies to the product of pulse amplitude and duty ratio $(V \cdot D)$.

With duty ratio control, the operation of the converter is then divided into the inner mode and outer mode (see Fig. 4), which is also described in [14]. To illustrate, Fig. 4 plots the idealized voltage and current waveforms $(D_2 = 0.5)$. The ZVS conditions are summarized in the figure.

B. Inner Mode

The inner mode takes place when the phase shift is small and means that the span of the voltage pulse $v_2^{'}$ is within v_1. The inner mode occurs when $|\varphi| < \varphi_B$, where φ_B is the boundary between the inner and outer mode:

$$\varphi_B = \frac{\pi}{2}(1 - D_2). \tag{6}$$

In this mode the current waveform i_1 (indicated in Fig. 3) exhibits a double-pulse shape. As shown in Fig. 4(a), in the first half period (t_0 to t_3) v_1 tends to increase the inductor current while $v_2^{'}$ tends to decrease it. If D_2 is controlled according to (5), the voltage-time integrals of v_1 and v_2' applied to the inductor L are equal from t_0 to t_3, that is

$$\frac{1}{L}\int_{t_0}^{t_3}(v_1 - v_2')dt = \frac{T}{2L}\left(V_1 - \frac{V_2 D_2}{n}\right) = 0 = \Delta i_1 \tag{7}$$

where T is the switching period. This is represented by the two shaded areas in Fig. 4(a). The difference between the inductor current at the start and end of the half cycle is equal to zero. Furthermore, since the inductor current is symmetrical, (that is, $i_1(t + 0.5T) = -i_1(t)$), together we have

$$\begin{cases} i_1(t_3) - i_1(t_0) = \Delta i_1 = 0, \\ i_1(t_3) = i_1(t_1 + 0.5T) = -i_1(t_0). \end{cases} \tag{8}$$

Solving the above equation gives

$$i_1(t_0) = i_1(t_3) = 0. \tag{9}$$

Therefore, in the idealized circuit the V_1-side bridge is critically zero-current switched (ZCS).

For the V_2-side bridge, switching occurs at t_1, t_2, t_4 and t_5. On the basis of (9), the current at the switching instants can be determined

$$\begin{aligned} i_1(t_1) &= \frac{V_1}{\omega L}(\varphi + \varphi_B), \\ i_1(t_2) &= \frac{V_1}{\omega L}(\varphi - \varphi_B). \end{aligned} \tag{10}$$

Because $|\varphi| < \varphi_B$ and the current is symmetrical, we can conclude that

$$\begin{aligned} &i_1(t_1) > 0, i_1(t_4) = i_1(t_1 + 0.5T) = -i_1(t_1) < 0; \\ &i_1(t_2) < 0, i_1(t_5) = i_1(t_2 + 0.5T) = -i_1(t_2) > 0. \end{aligned} \tag{11}$$

Therefore, the ZVS conditions are confirmed.

C. Outer Mode

The right-outer mode $(\varphi > \varphi_B)$ and left-outer mode $(\varphi < -\varphi_B)$ occur when the phase shift is large. For Fig. 4(b), the analytical expressions for the current at the commutating instants are calculated to be

$$\begin{aligned} i_1(t_0) &= -\frac{V_1}{\omega L D_2}(\varphi - \varphi_B), \\ i_1(t_1) &= \frac{V_1}{\omega L}(\varphi - \varphi_B), \\ i_1(t_2) &= \frac{V_1}{\omega L}(\varphi + \varphi_B). \end{aligned} \tag{12}$$

Because of the symmetry and the condition $\varphi > \varphi_B$, we have

$$\begin{aligned} &i_1(t_0) < 0, i_1(t_3) = i_1(t_0 + 0.5T) = -i_1(t_0) > 0; \\ &i_1(t_1) > 0, i_1(t_4) = i_1(t_1 + 0.5T) = -i_1(t_1) < 0; \\ &i_1(t_2) > 0, i_1(t_5) = i_1(t_2 + 0.5T) = -i_1(t_2) < 0. \end{aligned} \tag{13}$$

Therefore, the ZVS conditions for both V_1- and V_2-side are met. For the left-outer mode shown in Fig. 4(c), the same procedure applies and the conditions can also be verified.

Provided that the volt-second product of v_1 is equal to that of v_2', ZVS conditions are automatically achieved in the outer mode. In general, the switching condition is better in the outer mode than in the inner mode.

D. Power Flow Calculation

In the DAB converter, without duty ratio control the power flow is given by

$$P = \frac{V_1 V_2}{n\omega L}\varphi\left(1 - \frac{|\varphi|}{\pi}\right) \tag{14}$$

where φ is in radians, showing a nonlinear dependency on the phase shift.

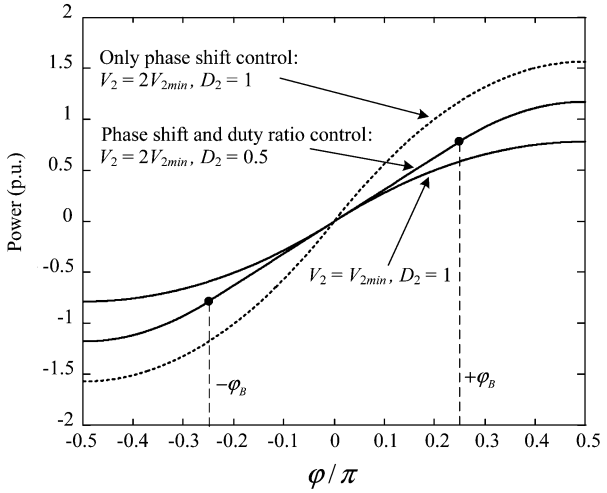

Fig. 5. Power flow versus phase shift in the DAB converter.

With the proposed duty ratio control method, the power flow is calculated to be

$$P = \begin{cases} \frac{V_1^2}{D_2\omega L}\left(\varphi\left(1-\frac{\varphi}{\pi}\right)-\frac{\pi}{4}\left(1-D_2\right)^2\right) & \text{if } \varphi > \varphi_B \\ \frac{V_1^2}{\omega L}\varphi & \text{if} |\varphi| \le \varphi_B \\ \frac{V_1^2}{D_2\omega L}\left(\varphi\left(1+\frac{\varphi}{\pi}\right)+\frac{\pi}{4}\left(1-D_2\right)^2\right) & \text{if } \varphi < -\varphi_B. \end{cases} \tag{15}$$

It is interesting to find that provided the transformer turns ratio is chosen according to (4) and the duty ratio is controlled by (5), the power flow for operation in the inner mode is a linear function of phase shift, while the power flow expression in the outer mode is nonlinear and complicated. Fig. 5 plots the power versus phase shift at different duty ratios. Due to the duty ratio control, less power is transferred at a given phase shift compared with that with only phase shift control.

III. Three-Port Topology

A. TAB Converter With Duty Ratio Control

The proposed duty ratio control method is not ideally suited for the two-port DAB converter because it does not guarantee ZVS over the full range of operation (only critical ZCS in the inner mode). However, ZVS conditions can be achieved in the three-port TAB converter.

Fig. 6 shows the topology of the converter for fuel cell and supercapacitor applications and its simplified model with bridges replaced by voltage sources. This configuration is identical to the TAB converter described in [11]. Conceptually, the circuit can be viewed as a network of inductors driven by voltage sources with controlled phase shifts. The power flow in the system is controlled by the phase shifts. The transformer is represented by a Δ-equivalent model to facilitate the system analysis [11]. The magnetizing inductance is neglected to simplify the analysis.

With the proposed duty ratio control method, ZVS conditions may be achieved over the entire phase shift region. The voltages of the fuel cell and the load are assumed to remain constant because the load voltage $V_{\rm Load}$ is regulated and the fuel cell is supposed to operate at constant power hence at a near-fixed operating voltage $V_{\rm FC}$. However, the supercapacitor operating voltage varies widely. Duty ratio control is applied to the supercapacitor side. Since the fuel cell and load side voltages are near-constant, we have

$$D_1 = D_2 = 1. \tag{16}$$

The transformer turns ratios, as indicated in Fig. 6, are chosen according to (in case of all full-bridges)

$$n_2 = \frac{N_2}{N_1} = \frac{V_{\rm Load}}{V_{\rm FC}}, n_3 = \frac{N_3}{N_1} = \frac{V_{\rm SC\,min}}{V_{\rm FC}} \tag{17}$$

where $V_{\rm SC\,min}$ is the minimum operating voltage of the supercapacitor; $V_{\rm Load}$ and $V_{\rm FC}$ are the voltages of the fuel cell and the load, respectively. Then, D_3 is controlled by

$$D_3 = \frac{V_{\rm SC\,min}}{V_{\rm SC}} \tag{18}$$

where $V_{\rm SC}$ is the supercapacitor operating voltage. The primary-referred amplitudes (peak values) of the voltages presented to the transformer and inductor network, as indicated in Fig. 6(c), are (for a full-bridge circuit) given by

$$V_1 = V_{\rm FC}, V_2' = \frac{V_{\rm Load}}{n_2}, V_3' = \frac{V_{\rm SC}}{n_3}. \tag{19}$$

Therefore, the following is true:

$$V_1 D_1 = V_2' D_2 = V_3' D_3. \tag{20}$$

Hence, the volt-second products of the three voltages applied to the corresponding transformer windings are equal. The reason why the converter is soft-switched lies in (20). This is explained as follows.

B. Analysis of ZVS Conditions

Thanks to the Δ-model representation, the system analysis is significantly simplified [11]. The three-port model is decomposed into three two-port models. The idealized operating waveforms of the TAB converter are illustrated in Fig. 7. Note that the waveforms vary with the operating point.

The ZVS condition for each bridge depends on the magnitudes of the currents at the switching instants. This is summarized in Fig. 7, in other words, negative currents at the v_1, v_2' and v_3' rising edges and positive currents at their falling edges. According to the definitions of the reference direction in Fig. 6(b), the instantaneous currents in the three branches are given by

$$\begin{aligned} i_1(t) &= i_{12}(t) - i_{31}(t), \\ i_2'(t) &= i_{23}(t) - i_{12}(t), \\ i_3'(t) &= i_{31}(t) - i_{23}(t). \end{aligned} \tag{21}$$

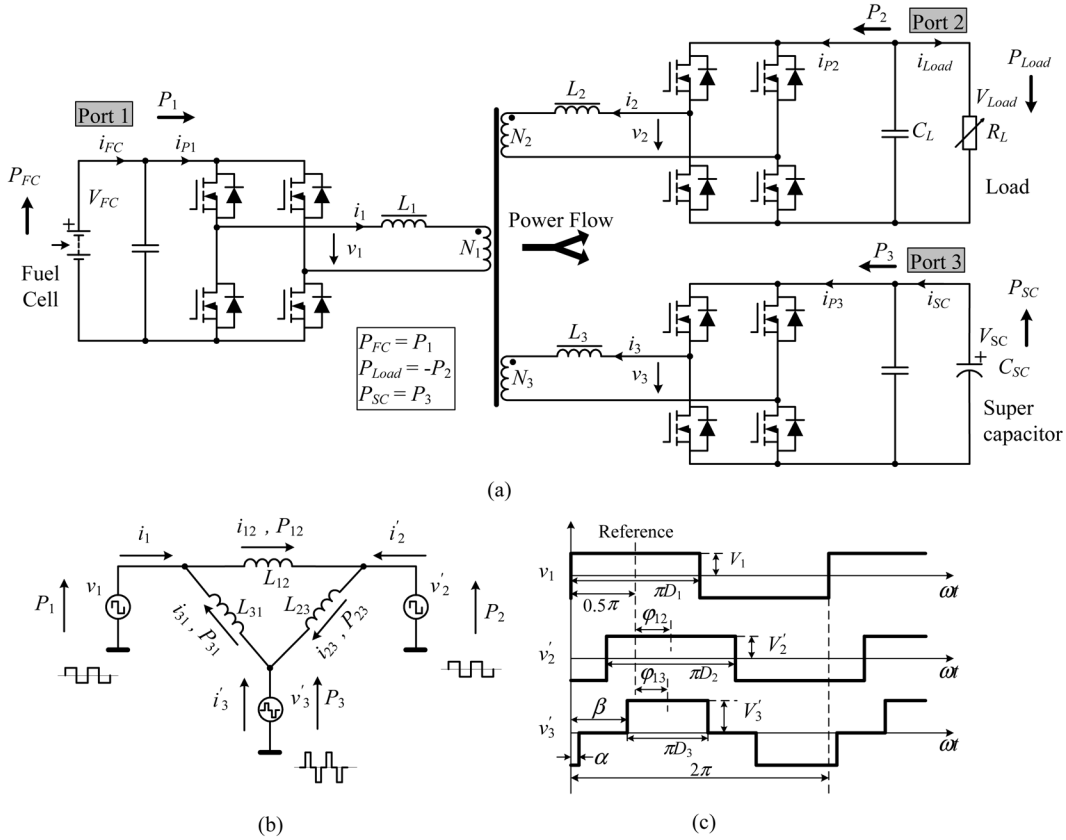

Fig. 6. TAB converter for fuel cell and supercapacitor application, showing (a) the TAB topology, (b) the primary-referred Δ-equivalent model, and (c) voltages generated by the three bridges shifted with φ_{12} and φ_{13} with v_1 as the reference. The angles α and β are defined for control purposes. The currents i_2', i_3' and the voltages v_2', v_3' represent the primary-referred values of i_2, i_3, v_2 and v_3, respectively.

Based on the analysis of the two-port topology, i_{31} and i_{23} will be exactly equal to zero at the switching (commutating) instants of v_1 and v_2' under idealized conditions (both-inner mode), i.e.,

$$\begin{aligned} i_{31}(t_0) &= i_{31}(t_4) = 0, \\ i_{23}(t_1) &= i_{23}(t_5) = 0. \end{aligned} \tag{22}$$

The voltage v_1 (fuel cell side) switches at t_0 and t_4, while at these two instants i_{31} equals zero. Therefore, the current of the fuel cell side bridge at the switching instants is

$$\begin{aligned} i_1(t_0) &= i_{12}(t_0) - i_{31}(t_0) = i_{12}(t_0), \\ i_1(t_4) &= i_{12}(t_4) - i_{31}(t_4) = i_{12}(t_4). \end{aligned} \tag{23}$$

So, i_{31} does not contribute to the ZVS condition of the bridge nor does it make the switching condition worse. The turn-off current of the bridge is only determined by i_{12} in the case shown. Because $V_{\rm FC}$ is assumed to be equal to $V_{\rm Load}/n_2$, the fuel cell side bridge is switched at zero-voltage in the entire phase shift region, as the optimal case $(d = 1)$ in the DAB converter [9].

An equivalent situation occurs at the load side bridge. For the supercapacitor side bridge, it switches under better ZVS conditions than the fuel cell and the load side bridges because both i_{23} and i_{31} contribute current to drive the soft-switched transition, as can be seen at t_2, t_3, t_6 and t_7 in Fig. 7.

For comparison, without duty ratio control hard-switching occurs at both the fuel cell and the load side bridge, as shown in Fig. 7 (dashed lines).

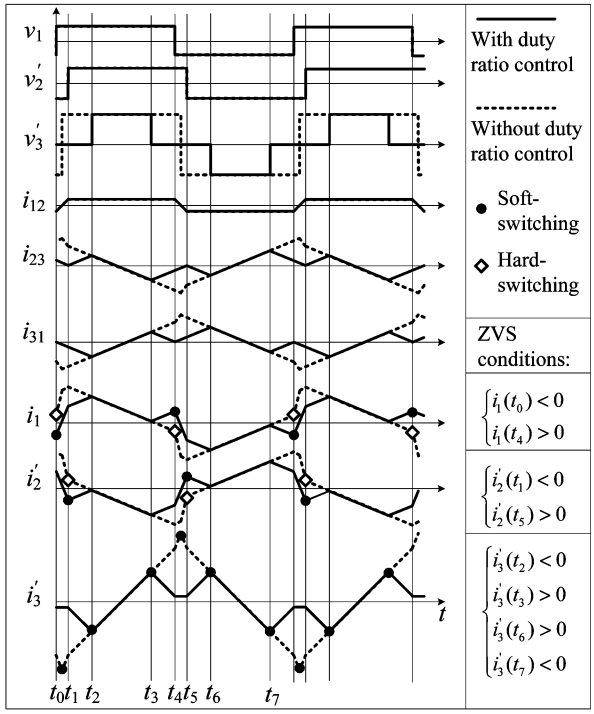

Fig. 7. Idealized steady-state operating waveforms of the TAB converter with and without duty ratio control in both-inner mode ($D_3 = 0.5, \varphi_{12} = 0.1\pi, \varphi_{13} = 0.05\pi, L_{12} = L_{23} = L_{31}$).

Similarly, other operating modes such as a combination of the inner and outer mode, or both-outer mode can be analyzed based

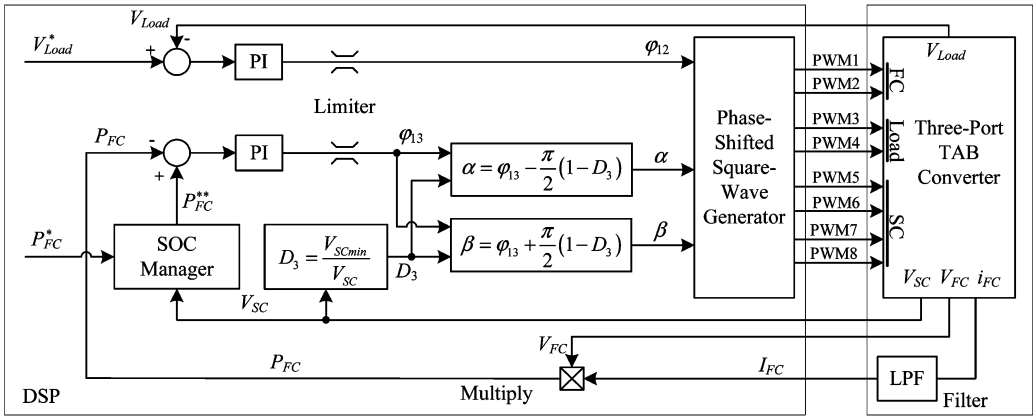

Fig. 8. Control scheme for the three-port TAB converter. $V^*_{\rm Load}$ and $P^*_{\rm FC}$ are the references for the output voltage and the fuel cell power, respectively.

on the results from the two-port topology. All of them switch under better ZVS conditions than the both-inner mode operation because all the three currents i_{12}, i_{23} and i_{31} contribute to soft-switching at the switching instants, based on the analysis of the two-port converter. In brief, provided that the current through each branch satisfies the ZVS condition, the combined current in two branches certainly assures ZVS operation. The worst case happens when both φ_{12} and φ_{13} equal zero. No real power would be transferred in this situation and two of the three bridges would be switched at zero-current in the ideal circuit.

In summary, because of the combination of currents in the three bridges, the proposed duty ratio control is effective in achieving ZVS in the three-port TAB topology. In the practical circuit the MOSFET drain-source capacitance and the magnetizing inductance of the transformer have to be considered. The MOSFET capacitance requires a minimum turn-off current and it reduces the soft-switched operating region. On the other hand, the magnetizing inductance will increase the soft-switching region and it compensates for the impact of the MOSFET capacitance [10].

IV. Control Strategy

A. DSP Control Scheme

A three-port system implies multiple control objectives. The proposed control scheme aims to regulate the output voltage $V_{\rm Load}$ and fuel cell power $P_{\rm FC}$ simultaneously. This strategy allows the load voltage to be tightly regulated, at the same time preventing load transients from affecting the operation of the primary source.

According to Fig. 6(c), there are three control variables, namely $\varphi_{12}, \varphi_{13}$ and D_3. Fig. 8 shows the DSP-based control scheme. The proposed control scheme has two PI (proportional-integral) feedback loops. The output voltage $V_{\rm Load}$ is regulated by φ_{12}. The fuel cell power $P_{\rm FC}$ is calculated by the multiplication of the measured voltage $V_{\rm FC}$ and the average current $I_{\rm FC}$, where the latter is obtained through a low-pass filter (LPF). Regulation of φ_{13} keeps the fuel cell power at the desired value. The adjustment of D_3 achieves ZVS. Since the supercapacitor voltage varies very slowly compared with the switching frequency, the duty ratio is nearly constant during many switching cycles.

Note that the control of D_3 is not intended to regulate the power flow. If the phase shifts were kept unchanged, the power flow in the system would vary when D_3 changes (see Fig. 5). In closed-loop operation, however, the power flow can be kept unchanged since the controller automatically adjusts the operating phase shifts in response to the change of the supercapacitor voltage. The change of the duty ratio D_3 may be viewed as a very slow disturbance to the control system.

The regulation of the fuel cell power is realized by a digital PI algorithm instead of feedforward control as proposed in [16].

For the implementation of the control scheme it should be noted that φ_{13} is not adjusted directly. Instead, as defined in Fig. 6(c), shift angles α and β are calculated by the DSP. They are found to be

$$\alpha = \varphi_{13} - \frac{\pi}{2}(1 - D_3),$$
$$\beta = \varphi_{13} + \frac{\pi}{2}(1 - D_3). \tag{24}$$

Note that the supercapacitor power is not controlled directly. The supercapacitor sinks or sources the balance of power between the fuel cell and the load automatically. An SOC manager monitors $V_{\rm SC}$. For instance, when the supercapacitor voltage approaches the maximum or minimum limiting voltage, the SOC manager slightly adjusts the fuel cell power reference. In this way the control circuit is capable of charging or discharging the supercapacitor with an average current

$$I_{\rm SC} = -(P^{**}_{\rm FC} - P_{\rm Load} - P_{\rm Loss})/V_{\rm SC} \tag{25}$$

where $I_{\rm SC}$ is the average discharging current, $P^{**}_{\rm FC}$ is the power reference given by the SOC manager, and $P_{\rm Loss}$ is the estimated total system loss.

B. System Modeling

To design the controller parameters for closed-loop operation, the small signal transfer function should be derived first. However, the conventional state space average model is not applicable for phase-shifted converters because the switching frequency is a possible control variable.

Averaged over one switching cycle, the DAB converter can be viewed as a dc current source whose amplitude is controlled by

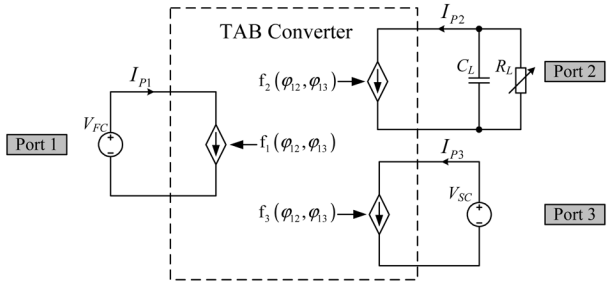

Fig. 9. Average model of the TAB converter.

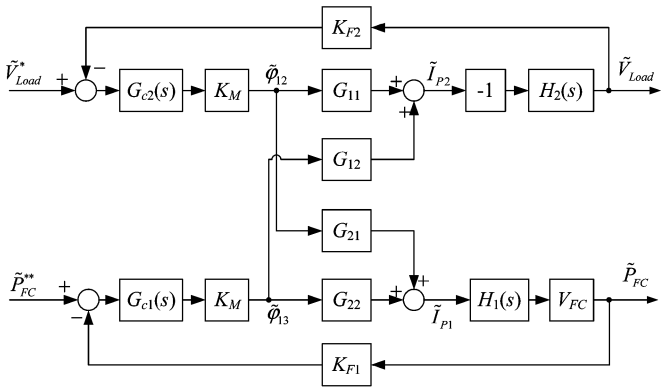

Fig. 10. Control loop block diagram of the TAB converter.

the phase shift [14]. Based on this approach the linearized small signal average model of the TAB converter can be derived. As shown in Fig. 9, the converter is modeled as three controlled dc current sources. Their amplitudes are controlled by the two phase shifts. The current source functions can be derived from the power flow equations as follows.

In the TAB converter the current at each port (i_{P1}, i_{P2} and i_{P3} [see Fig. 6(a)] can be averaged over one switching cycle. Let us denote the average values of i_{P1}, i_{P2} and i_{P3} by I_{P1}, I_{P2} and I_{P3}, respectively. They are functions of the two phase shifts, and are given by

$$\begin{aligned} I_{P1} &= \mathrm{f}_1(\varphi_{12},\varphi_{13}) = \frac{P_1}{V_{\mathrm{FC}}} \\ I_{P2} &= \mathrm{f}_2(\varphi_{12},\varphi_{13}) = \frac{P_2}{V_{\mathrm{Load}}} \\ I_{P3} &= \mathrm{f}_3(\varphi_{12},\varphi_{13}) = \frac{P_3}{V_{\mathrm{SC}}}. \end{aligned} \tag{26}$$

For an idealized three-port system, I_{P3} is redundant because $I_{P3} = -(I_{P1}V_{\mathrm{FC}} + I_{P2}V_{\mathrm{Load}})/V_{\mathrm{SC}} \cdot P_1, P_2$ and P_3 are functions of φ_{12} and φ_{13}. Note that D_3 is not regarded as a variable in the above equations because it changes very slowly and is not used to control the power flow. With the Δ-model the power flow at each port is a combination of power flow through two associated branches [see Fig. 6(b)]

$$\begin{aligned} P_1 &= P_{12} - P_{31}, \\ P_2 &= P_{23} - P_{12}, \\ P_3 &= P_{31} - P_{23}. \end{aligned} \tag{27}$$

Now the average current at each port can be obtained. The current source functions are nonlinear (because the power flow equations are nonlinear except for the inner mode) and thus should be linearized at the operating point for a control-oriented model. The factors of this linearization are derived by partial differentiation

$$\begin{aligned} G_{11} &= \left.\frac{\partial I_{P2}}{\partial \varphi_{12}}\right|_Q, \quad G_{12} = \left.\frac{\partial I_{P2}}{\partial \varphi_{13}}\right|_Q, \\ G_{21} &= \left.\frac{\partial I_{P1}}{\partial \varphi_{12}}\right|_Q, \quad G_{22} = \left.\frac{\partial I_{P1}}{\partial \varphi_{13}}\right|_Q. \end{aligned} \tag{28}$$

where $Q = (\varphi_{12o}, \varphi_{13o}, D_{3o})$ denotes the operating point. For example, for $D_3 = 1$, by using (14), (26) and (27), the linearized form of the average current at each port can be obtained

$$\begin{aligned} G_{11} &= -\frac{V_3}{n_2 n_3 \omega L_{23}}\left(1 - \frac{2}{\pi}|\varphi_{13o} - \varphi_{12o}|\right) \\ &\quad - \frac{V_1}{n_2 \omega L_{12}}\left(1 - \frac{2}{\pi}|\varphi_{12o}|\right), \\ G_{12} &= \frac{V_3}{n_2 n_3 \omega L_{23}}\left(1 - \frac{2}{\pi}|\varphi_{13o} - \varphi_{12o}|\right), \\ G_{21} &= \frac{V_2}{n_2 \omega L_{12}}\left(1 - \frac{2}{\pi}|\varphi_{12o}|\right), \\ G_{22} &= \frac{V_3}{n_3 \omega L_{31}}\left(1 - \frac{2}{\pi}|\varphi_{13o}|\right). \end{aligned} \tag{29}$$

Similarly, for D_3 different from 1, (15) can be used to calculate the small signal gain according to a given operating point; however, the expressions will be more complex. We can write the small signal gain of the TAB converter in matrix format

$$\begin{bmatrix} \tilde{I}_{P2} \\ \tilde{I}_{P1} \end{bmatrix} = \begin{bmatrix} G_{11} & G_{12} \\ G_{21} & G_{22} \end{bmatrix} \begin{bmatrix} \tilde{\varphi}_{12} \\ \tilde{\varphi}_{13} \end{bmatrix} = \mathbf{G_o} \begin{bmatrix} \tilde{\varphi}_{12} \\ \tilde{\varphi}_{13} \end{bmatrix} \tag{30}$$

where $\mathbf{G_o}$ denotes the gain matrix of the TAB converter.

Fig. 10 shows the control loop block diagram of the TAB converter, where $K_{F1} = 1$ and $K_{F2} = 1$ are the feedback gains and $K_M = \pi/3750$ is the gain of the DSP phase shift modulator. $G_{c1}(s)$ and $G_{c2}(s)$ are the transfer functions of the PI controllers

$$G_{c1}(s) = K_1\frac{1+\tau_1 s}{\tau_1 s}, G_{c2}(s) = K_2\frac{1+\tau_2 s}{\tau_2 s} \tag{31}$$

where $K_1 = 1$ and $K_2 = 50$ are the proportional gains and $\tau_1 = 0.5$ ms and $\tau_2 = 0.2$ ms are the time constants. The block with gain "-1" is due to the definition of the reference direction of i_{P2} in Fig. 6. The block with gain "V_{FC}" is needed because that the power is equal to the average current times the port voltage. $H_1(s)$ is the transfer function of the LPF which filters out ac components in i_{FC}

$$H_1(s) = \frac{1}{1+\tau_I s} \tag{32}$$

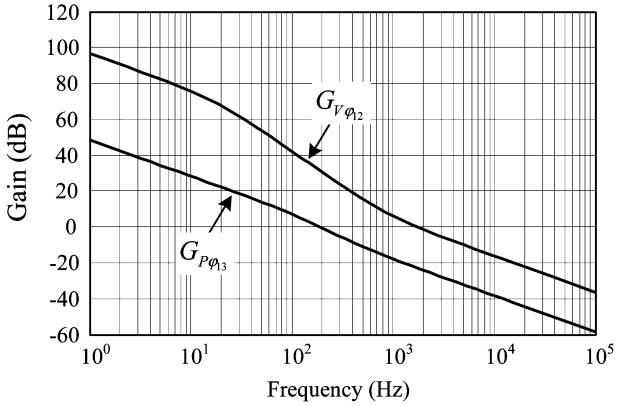

Fig. 11. Bode plot showing the open-loop gains of the system.

where $\tau_I = 1$ ms is the time constant of the filter. $H_2(s)$ is the transfer function of the output capacitor and load (supposed to be purely resistive)

$$H_2(s) = \frac{R_L}{1 + R_L C_L s} \tag{33}$$

where R_L is the resistance of the load and $C_L = 50\ \mu$F is the capacitance of the output filter capacitor.

For the TAB converter the main control variables φ_{12} and φ_{13} control the power flow in the system. In other words, two degrees of freedom are available for the system control. Not surprisingly, the two PI control loops are coupled and influence each other as can be seen from Fig. 10. The bandwidth of the output voltage control loop $G_{V\varphi_{12}}(s)$ is set higher than that of the power control loop $G_{P\varphi_{13}}(s)$ in order to guarantee a fast response to variations in load. In this manner the interaction can be minimized. One can regard the former controller as the master and the latter as the slave. This decoupling method is straightforward to implement. Fig. 11 plots the open-loop Bode plot of the two control loops, showing different crossover frequencies. The plotted transfer functions, using the parameters given above, are

$$\begin{aligned} G_{V\varphi_{12}}(s) &= -K_{F2} K_M G_{11} H_2(s) G_{c2}(s), \\ G_{P\varphi_{13}}(s) &= K_{F1} K_M V_{\mathrm{FC}} G_{22} H_1(s) G_{c1}(s). \end{aligned} \tag{34}$$

A further improvement would employ a decoupling network that eliminates the interaction effects. In theory, the decoupling matrix $\mathbf{D}$ is the inverse matrix of the TAB converter gain matrix $\mathbf{G}_o$ (i.e., $\mathbf{D} = \mathbf{G}_o^{-1}$) [12].

C. Methods for Soft Start-Up

Over-current at start-up is a drawback in both DAB and TAB converters. For instance, in the DAB converter the load side capacitor is charged from zero at start-up, while the source side is at its normal operating level. As a result, the current waveform is triangular having a high peak value. Furthermore, the load side bridge is hard-switched during this stage.

An easy way to avoid the over-current is to control the duty ratio of the source side bridge during start-up. Meanwhile the load side bridge is uncontrolled, effectively being a rectifier. By increasing the duty ratio gradually from zero to a certain value with open-loop control, the load side capacitor can be slowly charged to an operational level. Then, the closed-loop control takes over to regulate the output voltage. Note that the load should be disconnected from the output filter capacitor during the start-up procedure. For the TAB converter, the same procedure applies. A second method is to operate the converter at a higher frequency during the start-up. Because the impedance of inductor becomes higher at a higher frequency, the current is limited. In addition, a buck-boost start-up procedure for the TAB converter was discussed in [19].

V. Simulation and Experimental Results

A. Simulation Results

The TAB converter and its control scheme were simulated with PSIM. Parameters for the simulation are listed in Table I. Note that the fuel cell and load side bridges were implemented with half-bridges because they operate in square-wave mode. Fig. 12 shows the simulation waveforms of the voltages and currents in the three bridges in the cases of (a) a large $(D_3 = 1)$ and (b) a small $(D_3 = 0.5)$ duty ratio. As can be observed from Figs. 12(a) and 12(b), all the three bridges are soft-switched. On the contrary, in Fig. 12(c), without duty ratio control hard-switching occurs in two of the three bridges and the peak current is also much higher, where the operating parameters are the same as in the case of Fig. 12(b).

To verify the dual-PI-loop control scheme, Fig. 13 illustrates the power flow in the system in closed-loop operation, showing the step changes in the load power P_{Load} (between 1 and 2 kW) in a time interval of 10 ms, while the fuel cell power P_{FC} remains constant after the transitions.

It is advisable not to set the duty ratio D_3 less than 0.5. Otherwise the higher peak current will decrease the efficiency. The minimum supercapacitor voltage can be set to half of the rated/maximum voltage, i.e., a minimum duty ratio of 0.5. From the energy point of view, three quarters of the energy storage capacity of the supercapacitor is utilized because the energy is proportional to the square of the terminal voltage.

B. Experimental Results

The first laboratory prototype was rated at 1 kW maximum power at 20 kHz. The switching frequency is restricted by the resolution of the digitally implemented phase shift. It can be increased when using an analog controller, a DSP with high-resolution PWM output (e.g., TMS320F2808 DSP) or techniques such as dithering. A polymer electrolyte membrane (PEM) fuel cell with a maximum power 1 kW and a 145 F supercapacitor with a rated voltage of 42 V were used as the generator and storage, respectively. The fuel cell and load side bridges were implemented with half-bridges, and the supercapacitor side bridge was a full-bridge. Power MOSFETs were used as the switching devices for all the bridges. In the experimental prototype, the inductances are somewhat higher than the ones in the simulated circuit.

Fig. 14 $(D_3 = 1)$ and Fig. 15 $(D_3 = 0.5)$ show the measured voltages v_1, v_2 and v_3 generated by the bridges and the currents i_1, i_2 and i_3 through the transformer windings. It can be observed that the peak current is high when the duty ratio is

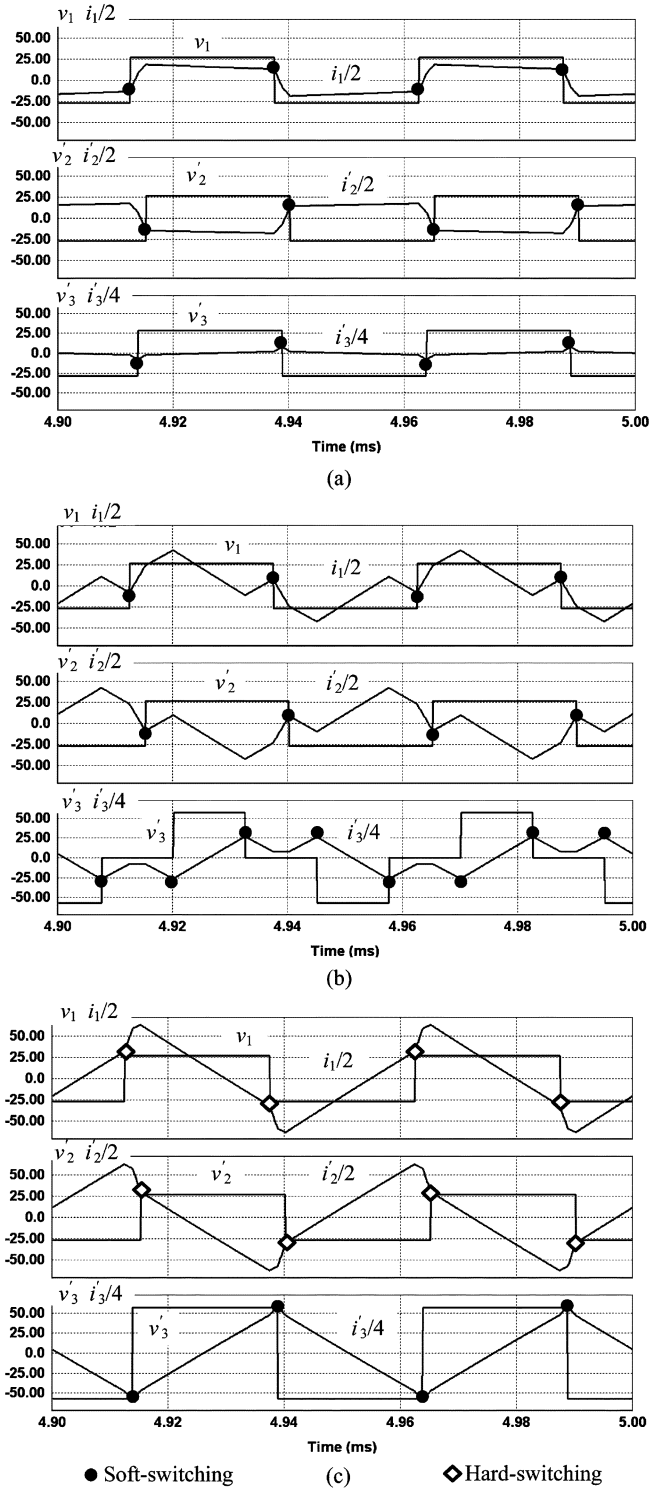

Fig. 12. Simulation results of the TAB converter at $\varphi_{12} = 0.1\pi$ and $\varphi_{13} = 0.05\pi$, showing soft-switching with duty ratio control at (a) $D_3 = 1$ and (b) $D_3 = 0.5$, and (c) hard-switching when not using duty ratio control at the supercapacitor side. Note that all waveforms are referred to the primary and the current waveforms are scaled.

small. Because of soft-switching, in both operating conditions the waveforms are clean and free of ringing.

Furthermore, system power flow control in response to a pulsating load under the closed-loop operation is illustrated in Fig. 16. The current (power) delivered by the fuel cell remains unchanged after the transients and the load variations are compensated for by the supercapacitor.

TABLE I
SYSTEM SIMULATION PARAMETERS

Description	Symbol	Value
Fuel cell voltage	V_{FC}	54 V
Load side dc voltage	V_{Load}	400 V
Supercapacitor voltage	V_{SC}	21 V to 42 V
Transformer turns ratio	$N_1 : N_2 : N_3$	5:38:4
Inductance	L_1	1.2 μH
Inductance	L_2	65 μH
Inductance	L_3	0.73 μH
Switching frequency	f_s	20 kHz

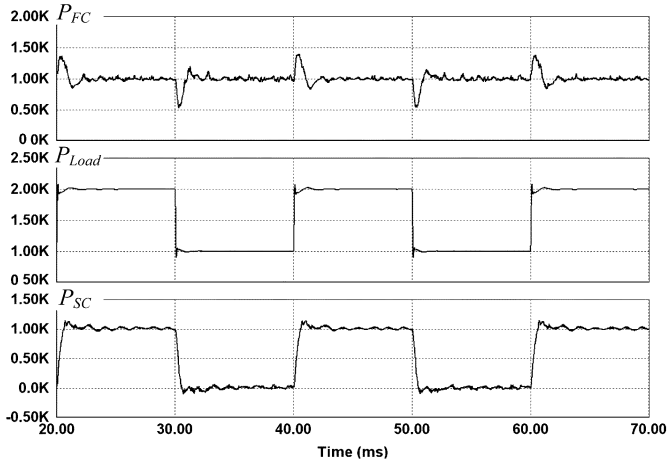

Fig. 13. Simulation results of the power flow control in response to step changes in the load.

A second prototype rated at 3.5 kW and 100 kHz switching frequency using all full-bridges was also successfully tested [20]. In this case the control scheme was implemented with the TMS320F2808 DSP (using high-resolution phase shift).

VI. DISCUSSIONS

In fact, fuel cells have a reasonably wide operating voltage depending on the output power. A duty ratio control method like the one for the supercapacitor can be applied to the fuel cell side

$$D_1 = \frac{V_{FC\,\min}}{V_{\rm FC}}, \quad D_2 = 1, \quad D_3 = \frac{V_{\rm SC\,min}}{V_{\rm SC}} \tag{35}$$

where $V_{FC\,\min}$ is the minimum operating voltage of the fuel cell. The transformer turns ratios are then chosen according to the minimum operating voltages, i.e.,

$$n_2 = \frac{N_2}{N_1} = \frac{V_{\rm Load}}{V_{FC\,\min}}, \quad n_3 = \frac{N_3}{N_1} = \frac{V_{\rm SC\,min}}{V_{FC\,\min}}. \tag{36}$$

It is possible to extend the three-port topology to an N-port topology—a multi-active-bridge dc–dc converter. According to the proposed method, the transformer turns ratios are chosen according to the minimum operating voltages at the ports

$$N_1 : N_2 : \cdots : N_N = V_{1\,\min} : V_{2\,\min} : \cdots : V_{N\,\min} \tag{37}$$

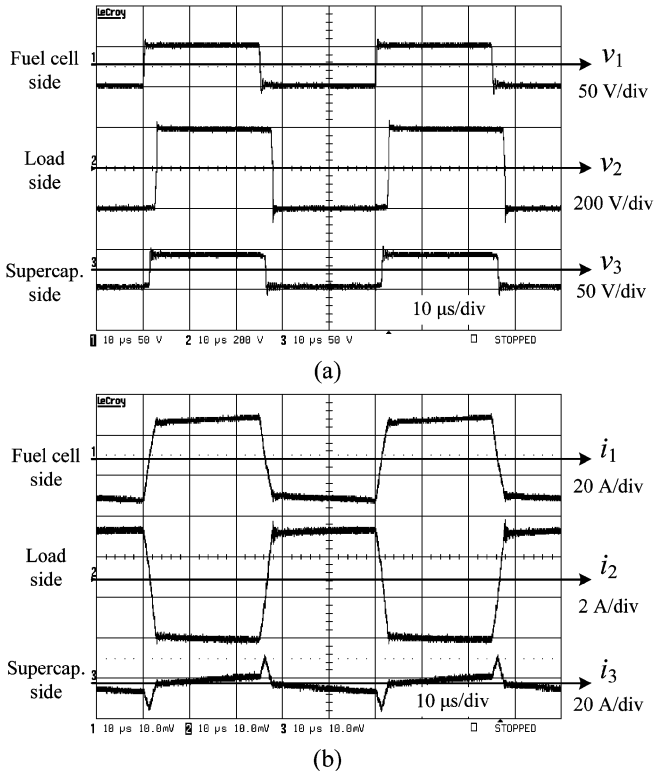

Fig. 14. Experimental results of the TAB converter at $\varphi_{12} = 0.1\pi, \varphi_{13} = 0.05\pi$ and $D_3 = 1$, showing (a) the voltages generated by the bridges, and (b) the currents through the transformer windings.

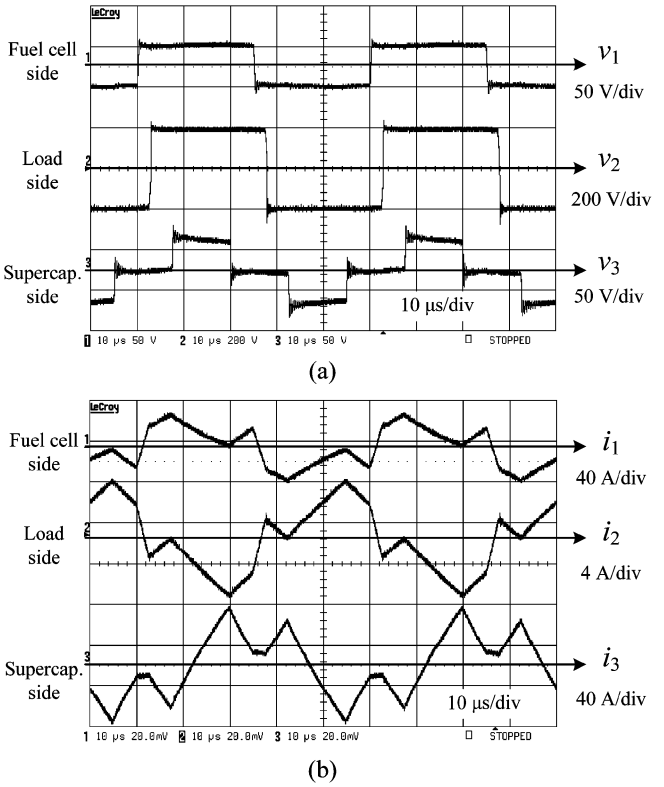

Fig. 15. Experimental results of the TAB converter at $\varphi_{12} = 0.1\pi, \varphi_{13} = 0.05\pi$ and $D_3 = 0.5$, showing (a) the voltages generated by the bridges, and (b) the currents through the transformer windings.

where $V_{1\min}, V_{2\min}, \ldots, V_{N\min}$ are the minimum operating voltages. The duty ratios are controlled with respect to the port operating voltages

$$D_1 = \frac{V_{1\min}}{V_1}, \quad D_2 = \frac{V_{2\min}}{V_2}, \ldots, D_N = \frac{V_{N\min}}{V_N}. \tag{38}$$

If the converter is controlled in this way, ZVS conditions for all the switches over the full operating region are theoretically achieved. The worst case is the critical ZCS. The advantage of the proposed duty ratio control method is that only a single division is needed to calculate the duty ratio.

VII. Conclusion

Sustainable energy generators such as fuel cells and storage like supercapacitors have a wide operating voltage range and therefore present optimization challenges for power converters. Neither the DAB nor the TAB converter can operate with soft-switching over the full operating region when the input voltage varies over a wide range. In addition to the primary power flow control that is achieved by phase-shifting the bridges, a simple and effective duty ratio control method has been proposed. Essentially, the latter aims to keep the volt-second product at each transformer winding equal. By adjusting the duty ratio of the voltage presented to the winding inversely proportional to the port dc voltage, ZVS conditions are achievable over the full operating range.

The application of this control method in a fuel cell and supercapacitor system has been analyzed. Duty ratio control is applied to the supercapacitor bridge and, if required, to the fuel cell bridge to handle voltage variations while maintaining ZVS. The system was modeled and a DSP-based dual-PI-loop control scheme was described in detail. This control scheme is straightforward to implement. The closed-loop simulation and experimental results of a 1 kW prototype validate the effectiveness of the converter and control strategy.

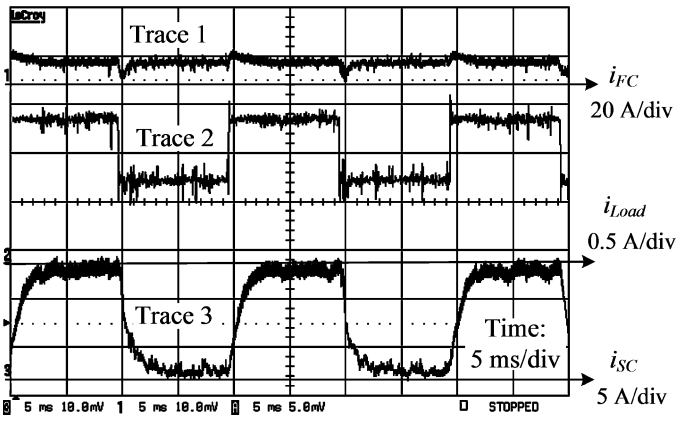

Fig. 16. Experimental results of the closed-loop power flow control of the TAB converter with the dual-PI-loop control scheme in response to step changes in the load.

References

[1] B. G. Dobbs and P. L. Chapman, "A multiple-input dc–dc converter topology," *IEEE Power Electron. Lett.*, vol. 1, no. 1, pp. 6–9, Mar. 2003.

[2] N. D. Benavides and P. L. Chapman, "Power budgeting of a multiple-input buck-boost converter," *IEEE Trans. Power Electron*, vol. 20, no. 6, pp. 1303–1309, Nov. 2005.
[3] H. Tao, A. Kotsopoulos, J. L. Duarte, and M. A. M. Hendrix, "Multi-input bidirectional dc–dc converter combining DC-link and magnetic-coupling for fuel cell systems," in *Proc. IEEE Ind. Appl. Soc. Conf. Annu. Meeting (IAS'05)*, Hong Kong, China, Oct. 2005, pp. 2021–2028.
[4] D. Liu and H. Li, "A ZVS bi-directional dc–dc converter for multiple energy storage elements," *IEEE Trans. Power Electron*, vol. 21, no. 5, pp. 1513–1517, Sep. 2006.
[5] H. Tao, A. Kotsopoulos, J. L. Duarte, and M. A. M. Hendrix, "Family of multiport bidirectional dc–dc converters," *Proc. Inst. Elect. Eng.*, vol. 153, no. 3, pp. 451–458, May 2006.
[6] H. Tao, A. Kotsopoulos, J. L. Duarte, and M. A. M. Hendrix, "Triple-half-bridge bidirectional converter controlled by phase shift and PWM," in *Proc. IEEE Appl. Power Electron. Conf. Expo (APEC'06)*, Dallas, TX, Mar. 2006, pp. 1256–1262.
[7] H. Al-Atrash, F. Tian, and I. Batarseh, "Tri-modal half-bridge converter topology for three-port interface," *IEEE Trans. Power Electron.*, vol. 22, no. 1, pp. 341–345, Jan. 2007.
[8] M. Marchesoni and C. Vacca, "New dc–dc converter for energy storage system interfacing in fuel cell hybrid electric vehicles," *IEEE Trans. Power Electron*, vol. 22, no. 1, pp. 301–308, Jan. 2007.
[9] R. W. De Doncker, D. M. Divan, and M. H. Kheraluwala, "A three-phase soft-switched high-power-density dc–dc converter for high-power applications," *IEEE Trans. Ind. Appl.*, vol. 27, no. 1, pp. 63–73, Jan./Feb. 1991.
[10] M. H. Kheraluwala, R. W. Gascoigne, D. M. Divan, and E. D. Baumann, "Performance characterization of a high-power dual active bridge DC-to-DC converter," *IEEE Trans. Ind. Appl.*, vol. 28, no. 6, pp. 1294–1301, Nov./Dec. 1992.
[11] M. Michon, J. L. Duarte, M. Hendrix, and M. G. Simoes, "A three-port bi-directional converter for hybrid fuel cell systems," in *Proc. IEEE Power Electron. Spec. Conf. (PESC'04)*, Aachen, Germany, Jun. 2004, pp. 4736–4742.
[12] C. Zhao and J. W. Kolar, "A novel three-phase three-port UPS employing a single high-frequency isolation transformer," in *Proc. IEEE Power Electron. Spec. Conf. (PESC'04)*, Aachen, Germany, Jun. 2004, pp. 4135–4141.
[13] K. Vangen, T. Melaa, S. Bergsmark, and R. Nilsen, "Efficient high-frequency soft-switched power converter with signal processor control," in *Proc. IEEE Telecommun. Energy Conf. (INTELEC'91)*, Nov. 1991, pp. 631–639.
[14] K. Vangen, T. Melaa, and A. K. Adnanes, "Soft-switched high-frequency, high power DC/AC converter with IGBT," in *Proc. IEEE Power Electron. Spec. Conf. (PESC'92)*, Jun. 1992, pp. 26–33.
[15] D. Xu, C. Zhao, and H. Fan, "A PWM plus phase-shift control bidirectional dc–dc converter," *IEEE Trans. Power Electron*, vol. 19, no. 3, pp. 666–675, May 2004.
[16] J. L. Duarte, M. Hendrix, and M. G. Simoes, "Three-port bidirectional converter for hybrid fuel cell systems," *IEEE Trans. Power Electron*, vol. 22, no. 2, pp. 480–487, Mar. 2007.
[17] H. Tao, A. Kotsopoulos, J. L. Duarte, and M. A. M. Hendrix, "A soft-switched three-port bidirectional converter for fuel cell and supercapacitor applications," in *Proc. IEEE Power Electron. Spec. Conf. (PESC'05)*, Recife, Brazil, Jun. 2005, pp. 2487–2493.
[18] H. Tao, A. Kotsopoulos, J. L. Duarte, and M. A. M. Hendrix, "Design of a soft-switched three-port converter with 0DSP control for power flow management in hybrid fuel cell systems," in *Proc. 11th Eur. Conf. Power Electron. Appl. (EPE'05)*, Dresden, Germany, Sep. 2005, pp. 1–10.
[19] C. Zhao, S. Round, and J. W. Kolar, "Buck and boost start-up operation of a three-port power supply for hybrid vehicle applications," in *Proc. IEEE Power Electro. Spec. Conf. (PESC'05)*, Recife, Brazil, Jun. 2005, pp. 1851–1857.
[20] H. Tao, J. L. Duarte, and M. A. M. Hendrix, "High-resolution phase shift and digital implementation of a fuel cell powered UPS system," in *Proc. 12th Eur. Conf. Power Electron. Appl. (EPE'07)*, Aalborg, Denmark, Sep. 2007, pp. 1–10.

Haimin Tao was born in China in 1976. He received the B.S. degree in electrical engineering and the M.S. degree in power electronics from Zhejiang University, Hangzhou, China, in 2000 and 2003, respectively, and the Ph.D. degree from the Eindhoven University of Technology (TU/e), Eindhoven, the Netherlands, in 2008.

From 2003 to 2004, he worked for Philips Lighting Electronics, Shanghai, China. Between 2004 and 2008, he carried out his Ph.D. research project at the TU/e. In January 2008, he joined Philips Lighting, Eindhoven. His current interests include power electronic con verters and digital control.

Andrew Kotsopoulos received the B.E. (with honors) degree and the Ph.D. degree in electrical and computer systems engineering from Monash University, Victoria, Australia, in 1992 and 1997, respectively. His Ph.D. thesis was in the area of soft-switched inverters.

After a period as a Research Assistant at Monash he spent two years as a Research and Development Engineer for an Australian inverter manufacturer. Between 2000 and 2005, he was with the Technical University of Eindhoven, Eindhoven, The Netherlands, as a Post-Doctoral Researcher in the Electrical Engineering Department. His research was related to power electronics in sustainable energy systems. In 2006, he joined ANCA Pty., Ltd., Bayswater North, Australia (a manufacturer of precision tool making machines based in Melbourne), where he is leading the development of new servo drive products. His interests include power electronic converters, digital signal processing and control systems.

Jorge L. Duarte (M'00) received the M.Sc. degree from the University of Rio de Janeiro, Rio de Janeiro, Brazil, in 1980 and the Dr.-Ing. degree from the Institut National Polytechnique de Lorraine (INPL), Nancy, France, in 1985.

He has been with the Electromechanics and Power Electronics Group, Technical University of Eindhoven, Eindhoven, The Netherlands, as a Member of the Scientific Staff, since 1990. During 1989, he was appointed a Research Engineer at Philips Lighting Central Development Laboratory, and since October 2000 he has also been a consultant Engineer at Philips Power Solutions, Eindhoven. His teaching and research interests include modeling, simulation and design optimization of power electronic systems.

Marcel A. M. Hendrix (M'98) received the M.S. degree in electronic circuit design from the Eindhoven University of Technology (TU Eindhoven), Eindhoven, The Netherlands, in 1981.

He is a Senior Principal Engineer at Philips Lighting, Eindhoven. In 1983, he joined Philips Lighting, Eindhoven, and started to work in the Pre-Development Laboratory, Business Group Lighting Electronics and Gear (BGLE&G). Since that time he has been involved in the design and specification of switched power supplies for both low and high pressure gas-discharge lamps. In July 1998, he was appointed a part-time Professor (UHD) with the Electromechanics and Power Electronics Group, TU Eindhoven, where he teaches design-oriented courses in power electronics below 2000 W. His professional interests are with cost function based simulation and sampled-data, nonlinear modeling, real-time programming, and embedded control.